ACS APPLIED MATERIALS & INTERFACES

Research Article

www.acsami.org

Tuning Molecular Weights of *Bombyx mori (B. mori)* Silk Sericin to Modify Its Assembly Structures and Materials Formation

Mingying Yang,*[,†,§] Yajun Shuai,[†,§] Guanshan Zhou,[†] Namita Mandal,[†] Liangjun Zhu,[†] and Chuanbin Mao*[,‡]

[†]Institute of Applied Bioresource Research, College of Animal Science, Zhejiang University, Yuhangtang Road 866, Hangzhou, 310058 Zhejiang, China

[‡]Department of Chemistry & Biochemistry, Stephenson Life Sciences Research Center, University of Oklahoma, 101 Stephenson Parkway, Norman, Oklahoma 73019-5300, United States

Supporting Information

ABSTRACT: *Bombyx mori (B. mori)* silk sericin is a protein with features desirable as a biomaterial, such as increased hydrophilicity and biodegradation, as well as resistance to oxidation, bacteria, and ultraviolet light. In contrast to other widely studied *B. mori* silk proteins such as fibroin, sericin is still unexplored as a building block for fabricating biomaterial, and thus a facile technique of processing it into a material is needed. Here, electrospinning technology was used to fabricate it into biomaterials from two forms of *B. mori* silk sericin with different molecular weights, one is a low (12.0 kDa) molecular sericin (LS) form and another is a high (66.0 kDa) molecular weight sericin (HS) form. Circular dichroism (CD) spectra showed that LS in hexafluoroacetone (HFA) solvent adopted a predominantly random coil conformation, whereas HS tended to form a β-sheet structure along with a large content of random coils. In addition, LS and HS in HFA solvent were found to form cylinder-like smaller nanoparticles and larger irregular aggregates before electrospinning, respectively. As a result, biomaterials based on microparticles and nanofibers were successfully fabricated by electrospinning of LS and HS dissolved in HFA, respectively. The cell viability and differentiation assay indicated that nanofibers and microparticles improved cell adhesion, growth, and differentiation, proving that the scaffolds electrospun from sericin are biocompatible regardless of its molecular weight. The microparticles, not common in electrospinning of silk proteins reported previously, were found to promote the osteogenic differentiation of mesenchymal stem cells in comparison to the nanofibers. This study suggested that molecular weight of sericin mediates its secondary structure and assembly structure, which in turn leads to a control of final morphology of the electrospun materials. The microparticles and nanofibers of sericin can be potentially used as building blocks for fabricating the scaffolds for tissue engineering.

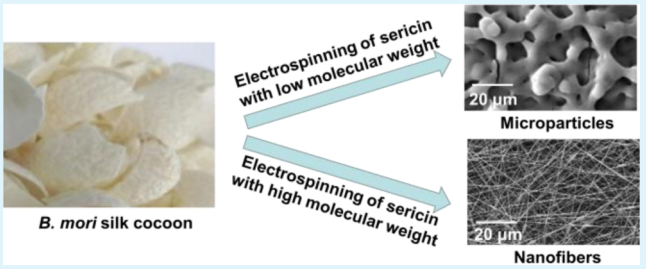

KEYWORDS: *Bombyx mori (B. mori) silk sericin, electrospinning, nanofibers, microparticles*

1. INTRODUCTION

Tissue engineering applies the principles of biology and engineering to the development of biological scaffolds for repairing damaged tissue and organs. The protein-based scaffolds hold promise in tissue engineering because natural extracelluar matrix are made of proteins.[1,2] Many proteins have been used to fabricate such scaffolds, such as collagen and silk-derived fibroin.[3−8] *B. mori* sericin, which is a global protein synthesized in the middle silk gland of *B. mori* silkworm, starts to receive attention as a potential scaffold in the field of tissue engineering due to its unique properties desired in biomedical applications. It has useful features such as resistance to oxidation, bacteria, and ultraviolet light and improved hydrophilicity and biodegradation.[9−11] It exhibits biological activities such as tyrosinase activity inhibition and pharmacological functions such as anticoagulation and anticancer.[12−15] Sericin contains a higher content of hydrophilic amino acids than fibroin, another silk-derived but well-studied protein. Thus, it has improved hydrophilicity and is easier to be chemically modified in comparison with the fibrion. However, unlike the already well-studied silk fibroin,[16−18] the actual biomedical application of sericin has not been fully explored due to the difficulty in processing it into useful materials.

Sericin is coated on the fibroin fiber when *B. mori* silkworm spins cocoon. It can be extracted by boiling cocoon in the elevated alkali and enzymatic solution or at conditions of high pressure and high temperature in water. In the processing of extraction, sericin is prone to degradation, which consequently results in significant decrease in the molecular weight down to below 20 kDa.[10] Its low molecular weight is the bottleneck

Received: May 23, 2014
Accepted: July 11, 2014
Published: July 22, 2014

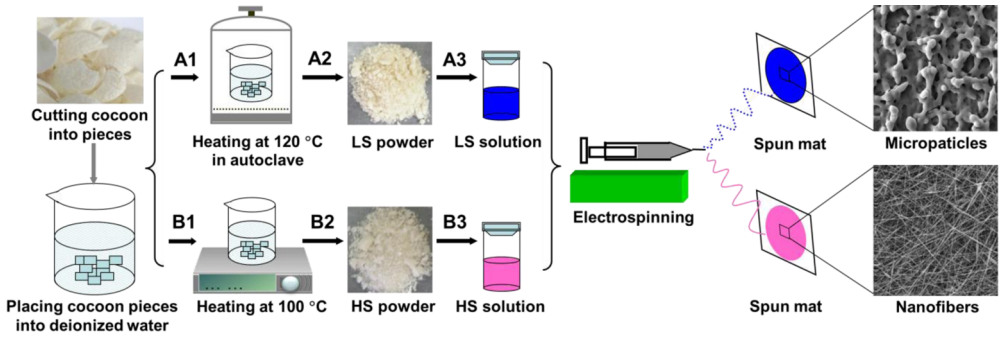

Figure 1. Proposed schematic for the fabrication of microparticles and nanofibers from sericin with different molecular weights by electrospinning. Cocoons were first cut into small pieces, which were placed into deionized water in a beaker. For the fabrication of microparticles, sericin powder with a low molecular weight (LS) was prepared (A1, A2), and LS solution for electrospinning was obtained by dissolving LS in HFA (A3). For the fabrication of nanofibers, sericin powder with high molecular weight (HS) was obtained (B1, B2) and then dissolved in HFA for nanofiber formation by electrospinning (B3). A1: cocoon pieces and deionized water were heated in an autoclave at 120 °C for 30 min to dissolve sericin from cocoon; A2: aqueous LS solution was extracted; A3: LS powder was dissolved in HFA at room temperature. B1: cocoon pieces were heated in deionized water at 100 °C for 10 min to obtain HS; B2: HS aqueous solution was extracted; B3: HS powder was dissolved in HFA at room temperature for electrospinning.

limiting its being processed into applicable forms. Although there have been reports on the formation of sericin nanofibers by directly dissolving sericin cocoon or powder in trifluoroacetic acid (TFA) as spinning dope for electrospinning,[19,20] the impact of molecular weight on the electrospinning ability of sericin is still unknown. In this work, we adopted a strategy of controlling protein-based materials formation through manipulating molecular weights of the precursor protein in electrospinning to fabricate the sericin protein into a material of well-defined morphologies.

Our previous research on electrospinning of recombinant silk proteins[21,22] shows that hexafluoroacetone (HFA) is an optimal solvent for the preparation of spinning dope. Thus, we anticipated that electrospinning of sericin might be successful by using HFA as a solvent. In addition, we assumed that molecular weight might play a role in the secondary structure and topography of sericin when dissolved in HFA solvent, which will in turn determine the morphologies of final materials through electrospinning.

Hence, this study attempted to fabricate microparticles and nanofibers to control the spun mat morphology by controlling the molecule weight of sericin followed by protein preassembly and electrospinning (Figure 1). Specifically, sericin with high (HS) and low (LS) molecular weights was prepared according to two different extraction conditions as described in Figure 1. After dissolved in HFA, HS and LS forms were expected to be assembled into different structures, which were electrospun into nanofibers and microparticles, respectively (Figure 1). Here for the first time, electrospinning technology was used to fabricate nanofibers or microparticles from *B. mori* silk sericin by changing its molecular weight. Since nanofibers or microparticles can serve as building blocks for fabricating scaffolds used in tissue engineering,[23−26] this work also investigates the biocompatibility by testing the cell viability on the matrix made from them.

2. MATERIALS AND METHODS

2.1. Materials. *B. mori* silkworm cocoons were purchased from the Shandong Academy of Sericulture, China. $CaCl_2$, Na_2HPO_4, and other chemical regents used here were of analytical grade and purchased from Sinopharm Chemical Reagents Co. Ltd., China. Deionized water was used throughout the experiment.

2.2. Preparation of LS and HS Powders. The sericin was prepared according to the reported procedure.[27] The detailed processing on extraction of LS and HS was described in Figure 1. *B. mori* silkworm cocoons were first cut into small pieces and placed into a beaker containing deionized water. For the preparation of LS, this beaker was heated in an autoclave with a temperature of 120 °C for 30 min to dissolve sericin. The aqueous sericin solution was collected. LS powder was obtained followed by lyophilization of aqueous sericin solution. In the case of HS, the beaker containing the cocoons in the deionized water was heated at 100 °C for 10 min, allowing sericin to be dissolved in the boiling deionized water. Then the aqueous sericin solution was gathered, followed by lyophilization of the solution to obtain HS powder.

2.3. Gel Permeation Chromatography (GPC) of LS and HS. The molecular weight distribution of LS and HS was measured using a liquid chromatography system (Agilent 1100, Agilent Technologies Inc., USA), equipped with a 15 × 25 mm column (Tricorn, GE Healthcare, USA). The GPC elution buffer was a phosphate buffer with a flow rate of 0.75 mL/min. Prior to the measurement, the aqueous LS or HS solution from the aforementioned experiment was centrifuged for 10 min at 6000 rpm to remove impurities. 100 μL of the aqueous LS or HS solution was loaded into the system at ambient temperature, and effluent solution was continuously monitored by UV detection at the wavelength of 280 nm. The molecular weight values from a calibration curve were obtained using protein standards. The amino acid analysis of LS and HS was performed using Hitachi L8900 Amino Acid Analyzer (Table S1).

2.4. Preparation of LS and HS Solution for Electrospinning. LS and HS solution used for electrospinning were prepared by dissolving LS and HS powders in HFA for 24 h at room temperature, respectively. The concentration of LS and HS solution ranged from 5 wt % to 10 wt %.

2.4.1. Circular Dichroism (CD) Spectroscopy of LS and HS Solution. CD spectra of LS and HS solutions were collected using a MOS-450 Spectrometer (Biologic, France). They were measured from 190 to 250 nm by using a quartz cell with a path length of 1 mm at the rate of 0.5 nm/s at room temperature. The concentration of LS and HS solution used for the CD measurement was 0.1 mg/mL. Each spectrum was the average value of four measurements. The spectra were smoothed and plotted in terms of residual molar ellipticity: $[\theta]M \times 10^{-3}$ ($deg \cdot cm^2 \cdot dmol^{-1}$).[28] A multiple Gaussian curve-fitting process was performed to quantify the area of each component. The relative percentage of the secondary structural elements was obtained from the area under the Gaussian curve by Origin 8.0.

2.4.2. Scanning Electron Microscopy (SEM), Atomic Force Microscopy (AFM) Observation, and Dynamic Light Scattering (DLS) Measurements. Three μL of LS or HS solution with a concentration of 0.01 mg/mL was deposited on the freshly exposed

mica surface and air-dried at room temperature. The morphologies of LS and HS solution were imaged by AFM (MultiMode, VEECO, USA). The morphologies of air-dried LS and HS were observed with SEM (S3000N, Hitachi, Japan). For SEM, the samples were mounted on aluminum stubs using adhesive carbon pads, sputter-coated with gold, and then examined under vacuum. For AFM, observation was performed at room temperature, and the images were taken using NanoScope Image. In addition, DLS measurements were performed for investigating the size distribution of LS and HS solution in HFA by using Zetasizer (Nano-ZS90, Malvern instruments, UK). The average particle size was obtained by measuring each sample in triplicate.

2.5. Electrospinning of LS and HS Solution. The electrospinning apparatus was constructed by a high voltage power supply (Gamma High Voltage Research Inc., USA), a syringe pump (Harvard Apparatus, USA), a 2 mL syringe, a stainless-steel needle (0.45 mm inner diameter), and a collecting plate (aluminum foil). The concentration of LS or HS in HFA was varied from 5 wt % to 10 wt % for obtaining spinning dopes with different viscosities. In the electrospinning process, a high electric potential was applied to a droplet of silk solution at the tip of a plastic capillary tubes. A voltage of 15 kV was applied by the high voltage power supply to inject the sericin solution onto the aluminum sheet. The flow rate of the LS or HS solution was 1.2 mL/h and controlled by the pump. The electrospun particles or fibers were collected on the aluminum sheet, which was placed at a distance of 15 cm from the tip of the plastic capillary tubes. The electrospinning apparatus was enclosed in a fume hood for removing harmful gases and drying electrospinning samples. All the as-spun samples were immersed in 90% (v/v) methanol aqueous solution for 12 h and then dried at room temperature.

2.6. Field Emission Scanning Electron Microscopy (FESEM) Observation of Microparticles and Nanofibers. The morphology of electrospun mats prepared from LS and HS, respectively, was observed using a FESEM (SIRON, FEI, Netherlands). Samples were dried and coated with gold before observing and imaging. In addition, the diameter distribution of nanofibers was calculated by using software Image-Pro Plus 6.0 coupled with Origin 8.

2.7. Fourier Transform Infrared Spectroscopy (FT-IR) and Thermal Gravimetric Analysis (TGA) of Microparticles and Nanofibers. The structure of microparticles and nanofibers before and after methanol treatment was measured with FT-IR. FT-IR spectra were recorded using a Fourier Transform Infrared Spectrometer (FTIR-8400S, Shimadzu, Japan). A total of 2 mg samples were mixed with 200 mg of KBr and then pressed into discs, respectively. The measurements were performed with the wavenumber ranging from 400 to 4000 cm^{-1}. Thermal behavior of microparticles and nanofibers, before and after methanol post-treatment, was performed on simultaneous differential thermal and thermal gravimetric analyzer (DTA-TG, Shimadzu Corporation, Japan). All the samples were ground into powder and then loaded in an aluminum crucible under dry conditions. DTA-TG measurement was performed in a nitrogen atmosphere with temperature ranging from 50 to 400 °C at a heating rate of 10 °C/min.

2.8. Cell Morphology and Cell Viability Assay. Cell culture was performed by using HEK-293 cells. Cells at the third or fourth passage were used in this study. The electrospun mats including microparticles and nanofibers were fixed on the wells of microplates. Each well was sterilized by 75% (V/V) ethanol and washed with physiological saline three times. Cells were cultured in DMEM with 10% FBS and 1% penicillin–streptomycin. Cells at a seeding density of 1.0×10^4 cells/cm^2 were immediately placed in an incubator at 37 °C, 5% CO_2. The cells were counted using Scepter hand-held automated cell counter (Millipore, USA). Moreover, another cell, MG-63 cells, was also used as a testing cell to evaluate the cell viability of these two electrospun mats.

2.8.1. Cell Morphology. After the cells were cultured for 1 and 5 days, their morphology was observed according to the following steps: Cells were first fixed in 2.5% glutaraldehyde in a phosphate buffer saline (PBS, pH 7.0) for 4 h, then fixed with 1% OsO_4 in PBS for 1 h, and washed 3 times by PBS. After that, the fixed specimens were dehydrated by increasing the concentration of ethanol from 30%, 50%, 70%, 80%, 90%, 95% to final 100%, and the time for each step was about 20 min. The dehydrated specimens were immersed in iso-amyl acetate for about 1 h and allowed to dry overnight in Hitachi Model HCP-2 critical point dryer with liquid CO_2. After drying, the specimens were mounted on the aluminum stubs, sputter-coated with gold, and observed in a Philips Model TM-1000 SEM.

2.8.2. MTS Assay. The cell viability on electrospun mats was determined by using Cell Titer 96 Aqueous One Solution cell proliferation (MTS) assay according to the manufacturer's protocol (Promega). The HEK-293 cells were cultured on the electrospun mats for 1, 3, and 5 days. Subsequently, 20 μL of MTS compound solution was added to each specimen and incubated for 3 h in a 5% CO_2 incubator at 37 °C. The optical density (OD) at the wavelength of 490 nm, reflecting the number of cells, was measured using a microplate reader (Bio-Rad 680).

3. RESULTS AND DISCUSSION

3.1. Molecular Weight of LS and HS. The GPC is a useful and powerful method to determine the apparent molecular weight of a protein.[29] Figure 2 showed the GPC traces of LS,

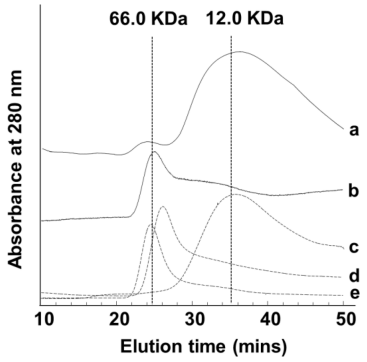

Figure 2. GPC profile of molecular weight distribution of sericin powders and three molecular weight markers. The samples of (a), (b), (c), (d), and (e) are LS powder, HS powder, RNase A, subunit of catalase, and bovine serum albumin, respectively.

HS, and three molecular weight markers (bovine serum albumin: 66.4 kDa, subunit of catalase: 60.0 kDa, and RNase A: 13.7 kDa). According to the molecular weight markers, the most frequent molecular weight distribution of LS was mainly centered at 12.0 kDa with a minor distribution at 66.0 kDa, while the molecular weight of HS was mainly distributed at 66.0 kDa. Although the molecular weight of HS was significantly higher than that of LS, the amino acid composition of LS and HS showed no significant difference (Table S1). This indicates that preparation conditions including temperature, pressure, and heating duration can largely mediate the molecular weight of sericin when it is extracted from cocoons. Namely, the molecular weight of sericin can be controlled by controlling the extraction conditions.

3.2. Assembly Structure of LS and HS in Solvent HFA. To investigate the effect of molecular weight and solvent on the assembly structure of sericin, LS and HS dissolved in HFA were characterized at room temperature with CD measurement. HS and LS displayed distinct CD spectral patterns (Figure 3). The curve fitting analysis of the CD profiles indicated that LS adopted a β-sheet conformation at a content of 58% with the rest secondary structure being random coil structures according to the appearance of two negative peaks at 200 and 216 nm (Figure 3A).[30,31] However, HS mainly formed β-sheet structure, which was judged by a strong negative peak at 218 nm corresponding to β-sheet conformation (Figure 3B).[32]

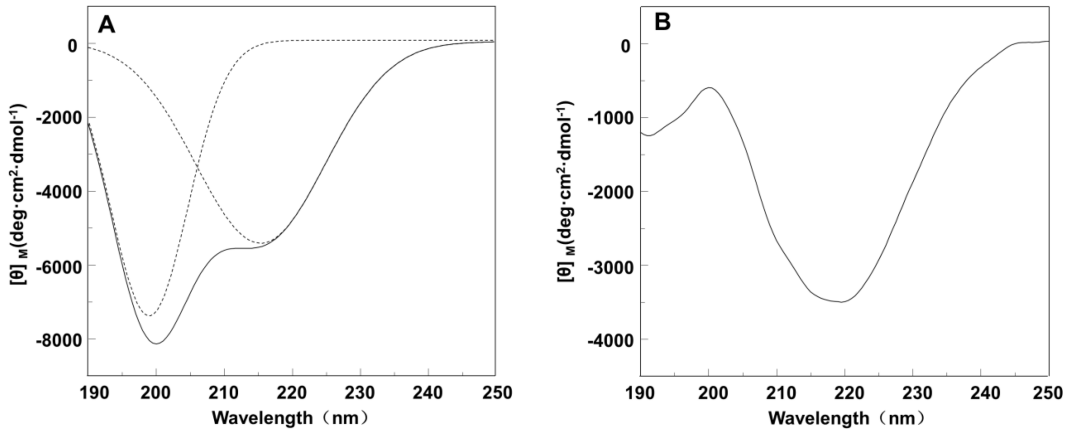

Figure 3. CD spectra of sericin with different molecular weights in HFA solvent (0.1 mg/mL). (A) LS solution. Dotted lines are results of the curve fitting. (B) HS solution.

Furthermore, both LS and HS dissolved in HFA formed structures different from those dissolved in water.[33]

SEM observation showed that LS and HS dissolved in HFA were assembled into different morphologies (Figure 4). LS

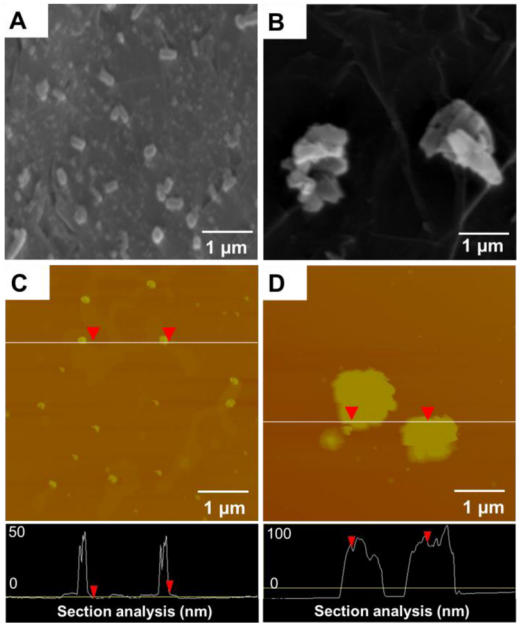

Figure 4. Nanostructures assembled from sericin with different molecular weights in HFA solutions. A and C are LS solution, and B and D are HS solution. A and B are SEM images. C and D are AFM images. The AFM section profile measurements of HS and LS are shown at the bottom of AFM image (black areas). The corresponding position of the black area is shown with red arrows and a white line in the original AFM images (C and D).

formed cylinder-like particles with a size of 200−300 nm, which were independently scattered on the surface of mica (Figure 4A). In contrast to LS, HS was aggregated into larger particles (about 1 μm) without a well-defined morphology (Figure 4B). AFM images also showed that LS and HS formed particles with an average diameter of about 200 nm (Figure 4C) and 800 nm (Figure 4D), respectively. The images at the bottom of AFM images represented a section profile of LS and HS in the position indicated by red arrows and white lines, respectively. The section profile demonstrated that the height of LS particles was 40−55 nm, and that of HS was 90−110 nm. The size of the particles assembled from the same protein revealed by SEM and AFM is slightly different probably because the samples imaged by AFM and SEM were wet and dry, respectively. Moreover, DLS was used to observe LS and HS dissolved in HFA directly (Figure S1). Although DLS data showed that the hydrodynamic sizes of LS and HS particles in HFA solution were different from those determined by AFM or SEM imaging, it indicated that the particle size of LS was smaller than that of HS when both of them were dissolved in HFA (Figure S1). Collectively, SEM and AFM as well as DLS all proved that a higher molecular weight resulted in larger sericin particles.

Therefore, CD spectra as well as SEM and AFM images proved that molecular weight can determine the assembly structure of sericin dissolved in HFA. The low molecular weight favors the formation of the β-sheet and random coil conformation of LS, which leads to the weak molecular interaction between LS and the consequent assembly into cylinder-like particles due to its short molecular chain. In contrast, high molecular weight favors the formation of β-sheet structure of HS in HFA, which probably promotes the aggregation of HS into larger particles due to its heavy cross-linking nature. Therefore, this result implies that molecular weight might impact electrospinning ability of sericin and the morphology of electrospun mats.

3.3. Fabrication of Microparticles. Figure 5 showed the FESEM morphology of microparticles spun from the HFA solutions of LS with the concentrations of 5, 7.5, and 10 wt %, reflecting the different viscosity. No obvious microparticles were observed in the concentration of 5 and 7.5 wt % (Figure 5A, B). When the concentration was increased to 10 wt %, spherical microparticles were observed and aggregated into clusters (Figure 5C). After methanol treatment, spherical microparticles were found on all three concentrations of LS, and microparticle arrangement of those electrospun mats was different at different concentrations of LS (Figure 5D−F). From Figure 5G−I (enlarged Figure 5D−F), it was clearly seen that aggregation of particles was increased with increase in the concentration; however, the size of particles remained to be about 1.5 ± 0.3 μm. This indicated that micropartcles can be obtained using electrospinning of sericin with low molecular weight, and the topography of the microparticle mats was also mediated through arrangement of microparticles by controlling the concentration of sericin and post-treatment.

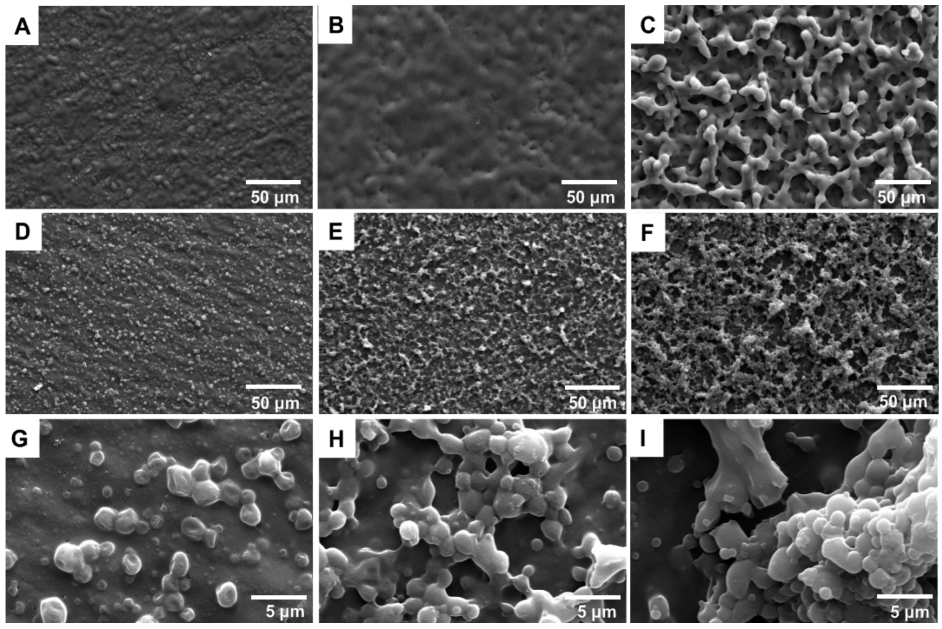

Figure 5. FESEM images of microparticles prepared from LS with the concentration of (A) 5 wt %, (B) 7.5 wt %, and (C) 10 wt %. (D), (E), and (F) are samples corresponding to (A), (B), and (C) after treatment with methanol, respectively. (G), (H), and (I) are high magnification images corresponding to (D), (E), and (F), respectively.

3.4. Fabrication of Nanofibers. Nanofiber formation of HS was attempted with various viscosity by changing the concentration from 5 wt %, through 7.5 wt %, to 10 wt %. The FESEM image (Figure 6A) indicated that nanofibers could not

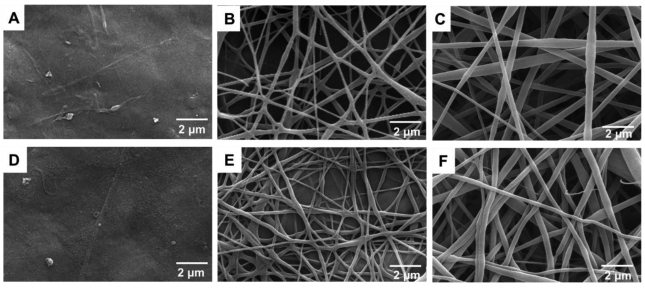

Figure 6. FESEM images of nanofibers prepared from HS with the concentration of (A) 5 wt %, (B) 7.5 wt %, and (C) 10 wt %. (D), (E), and (F) are samples corresponding to (A), (B), and (C) after treatment with methanol, respectively.

be formed from HFA solution with a concentration of 5 wt %. When the concentration was increased to 7.5 and 10 wt %, nanofibers were obtained (Figure 6B, C). The diameter of the nanofibers was increased with the increase in the concentration. After methanol treatment, still no nanofibers were observed in the case of concentration with 5 wt %, and the fine fibers in Figure 6E, F aggregated to form thick fibers by network formation, contrary to previous report on nanofibers prepared from fibroin.[22] The diameter distribution of fibers is shown in Figure 7. The diameter of nanofibers prepared from 7.5 wt % ranged from 50 to 600 nm, and the mean diameter was 244 nm (Figure 7A). In the case of 10 wt %, the diameter varied from 100 to 650 nm, and the mean diameter of nanofibers was about 339 nm (Figure 7B). After methanol treatment, the average diameter of both nanofibers was decreased to 179 and 312 nm, respectively (Figure 7C, D). It can be seen that the diameter of nanofibers can be controlled by the HS concentration and post-treatment.

3.5. The Structural Characteristic and Thermal Behavior of Microparticles and Nanofibers. In order to investigate the impact of molecular weight and post-treatment on the secondary structures of microparticles and nanofibers prepared from LS and HS solutions, FT-IR analysis was carried out (Figure 8A). The amide I vibration arises mainly from the C═O stretching vibration. It depends on the secondary structure of the backbone. However, the amide II is the out-of-phase combination of the NH in-plane bending. Hence, the amide II was used as an evidence to detect the structural characterization of microparticles and nanofibers. After methanol treatment, the central peak of amide II of microparticles and nanofibers was transited from 1540 to 1525 cm^{-1}, indicating that methanol treatment favored the β-sheet conformation of sericin. Although CD spectra indicated the difference between LS and HS in HFA solution, FT-IR spectra did not detect significant difference in the secondary structures between microparticles and nanofibers due to the disappearance of the interaction with HFA. However, DTA curves showed that before methanol treatment, microparticles and nanofibers had different behaviors of thermal decomposition and phase changes (Figure 8B) with microparticles having one endothermic peak at 175.8 °C whereas nanofibers having two endothermic peaks at 175.8 and 197.1 °C. After methanol treatment, one endothermic peak at 197.1 °C was observed on microparticles and nanofibers. These results suggested that microparticles and nanofibers showed similar secondary structure and thermal behaviors after methanol treatment.

3.6. Cell Viability on Microparticles and Nanofibers. Figures 9A–D showed the SEM micrographs of HEK 293 cells attached and grown on the electrospun mats. After cultured for 1 day, HEK 293 cells on the microparticle mats were globular and aggregated (Figure 9A), whereas those cultured on the nanofiber mats spread with an elliptical morphology (Figure

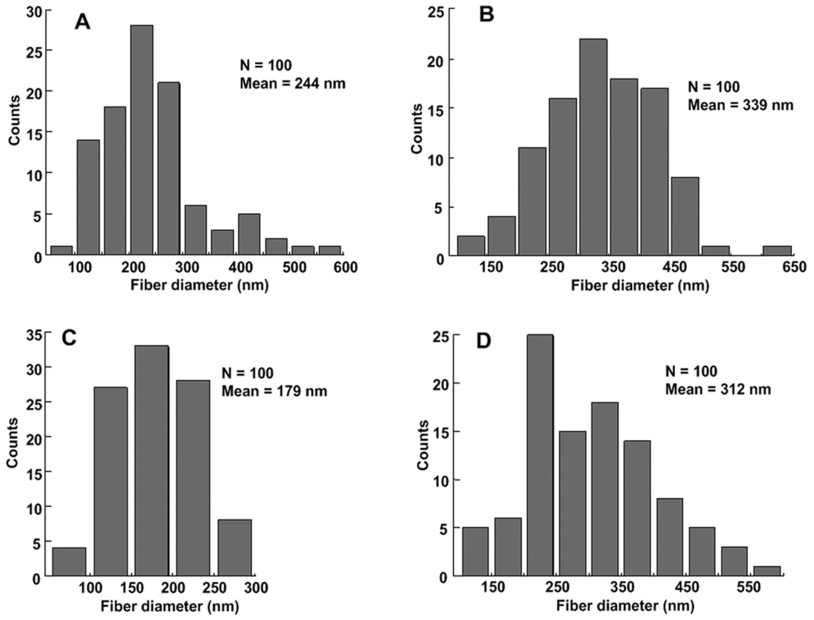

Figure 7. Histograms of nanofiber diameter distribution. (A) 7.5 wt %, (B) 10 wt %, (C), and (D) are samples corresponding to (A) and (B) after treatment with methanol, respectively.

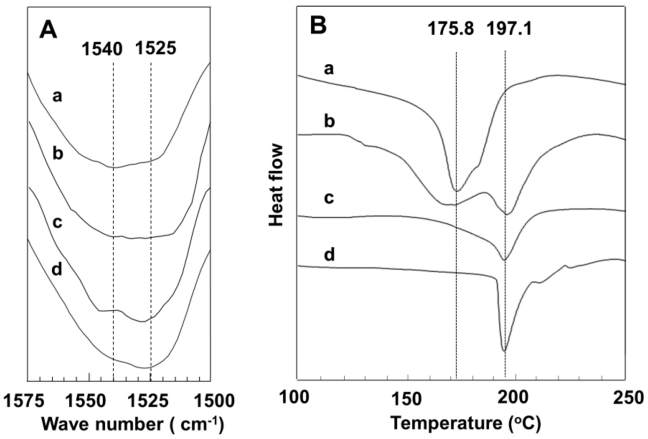

Figure 8. FTIR spectra (A) and TGA curves (B) of microparticles and nanofibers. (a) microparticles prepared from LS with a concentration of 10 wt %; (b) nanofibers prepared from HS with a concentration of 10 wt % . (c) and (d) are samples corresponding to (a) and (b) after treatment with methanol, respectively.

9B). After cultured for 5 days, multilayers of HEK 293 cells covered both microparticle and nanofiber mats (Figure 9C, D). A similar tendency was observed on the MG-63 cells attached and grown on the electrospun mats (Figure S2). Especially, the bridges and short pseudopods of cells were observed among the elongated cells on nanofiber mats. SEM observation indicated that cells could be attached onto the microparticle and nanofiber mats, and the cell attachment was more favored on the nanofibers in the early period of culture.

Moreover, MTS analysis confirmed that the proliferation rate on nanofiber mats was higher than on microparticle mats. The proliferation of HEK 293 cells on nanofiber mats was faster than on microparticle mats on day 1, 3, and 5 (Figure 9E). After the cells were cultured for 5 days, their number increased significantly ($p < 0.01$) on the nanofiber mats compared to microparticle mats. The proliferation rate of the MG-63 cells was also higher on the nanofiber mats than on microparticle mats (Figure S2−F). The results of MTS assay indicated that the electrospun sericin mats in the form of nanofibers could accelerate the proliferation of HEK 293 cells.

3.7. Cell Differentiation on Microparticles and Nanofibers. We followed our published protocols[34,35] to evaluate the osteogenic differentiation of rat mesenchymal stem cells (MSCs) on the microparticle and nanofiber scaffolds in the osteogenic differentiation media. Specifically, alkaline phosphatase (ALP) and osteocalcin (OCN), representing the early and late stage of the osteogenic differentiation of MSCs, were detected by ALP assay and real-time polymerase chain reaction (PCR) analysis, respectively. ALP assay (Figure S3) showed that the ALP activity of MSCs on both forms of electrospun sericin materials were significantly higher than the tissue culture plate ($p < 0.01$), suggesting that the electrospun sericin promoted the osteogenic differentiation of MSCs in comparison with the substrate without sericin materials. In addition, it demonstrated that microparticle sericin scaffolds had a higher capacity in promoting the osteogenic differentiation than the nanofiber sericin scaffolds (Figure S3). Moreover, real-time PCR analysis (Figure S4) showed that OCN gene expression level of MSCs on both microparticles and nanofibers scaffolds was significantly higher than that on the tissue culture plate ($p < 0.01$), further indicating that the electrospun sericin scaffolds promoted the osteogenic differentiation of MSCs. It also demonstrated that the microparticles scaffolds are more effective in enhancing the osteogenic differentiation of MSCs, consistent with the ALP assay. Therefore, our data show that the electrospun sericin scaffolds can significantly promote the osteogenic differentiation of MSCs. Furthermore, our study was the first example showing that electrospinning could fabricate sericin into a new form, microparticles, in addition to the traditional nanofibers. Since microparticle scaffolds showed a higher capacity in promoting osteogenic differentiation of MSCs, our work, by tuning the molecular weights of the sericin, resulted in a new type of sericin materials that can find potential applications in bone tissue engineering.

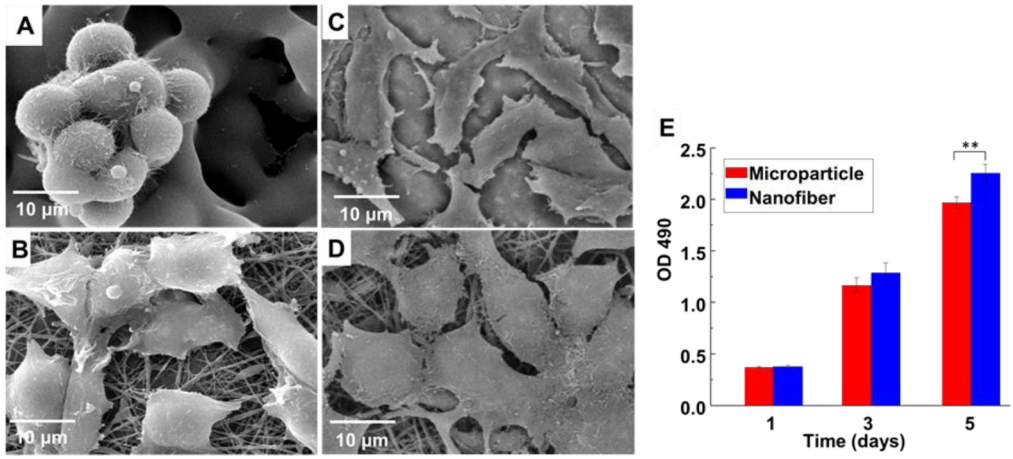

Figure 9. Morphology and proliferation of HEK 293 cells on electrospun mats. Morphology of HEK 293 cells on (A, C) microparticle mats and (B, D) nanofiber mats after cultured for (A, B) 1 day and (C, D) 5 days. Proliferation of (E) HEK 293 cells on the electrospun mats determined using MTS assay. **, $p < 0.01$.

We have shown that microparticles and nanofibers were obtained from LS and HS by dissolving them in HFA followed by electrospinning, respectively. We also discovered that molecular weight determined not only its secondary structure (Figure 3) but also its topography in HFA (Figure 4). Finally, the molecular weight of sericin affected the morphology of sericin spun mat (Figures 5 and 6). LS only formed small particles (Figure 4A, C) that could not be cross-linked with each other due to its low molecular weight. Consequently, these small particles were organized into microparticles by electrospinning as anticipated by Figure 1 and proved by Figure 5. In contrast to LS, HS first formed large particles (Figure 4B, D) through supramolecluar assembly as a result of high molecular weight, and these particles could be pushed into fibers by electric force (Figures 1, 6, and 7). Therefore, LS and HS form different precursor structures in solution before electrospinning, which will lead to the formation of different structures after electrospinning. The microparticles and nanofibers showed similar secondary structure and thermal behaviors (Figure 8). The results from cell viability and differentiation assay proved that microparticles and nanofibers prepared from sericin were biocompatible and could serve as building blocks for the fabrication of bone tissue engineering scaffolds (Figure 9). Therefore, this study found out that mediating molecular weight of sericin is a simple strategy to control the morphology of electrospun sericin scaffolds in the form of either microparticles and nanofibers.

4. CONCLUSIONS

In order to develop biomaterials based on sericin, this study attempted to process sericin into useful forms including microparticles and nanofibers that can serve as building blocks in the assembly of scaffolds for tissue engineering. This study is the first time to obtain microparticles and nanofibers from sericin by using HFA as a solvent for the preparation of spinning dope in the processing of electrospinning. It suggests that the molecular weight can determine its assembly structure in solution state and consequently influence the topography of electrospun mats. The low molecular weight weakening the cross-linking of sericin results in microparticles, whereas high molecular weight accelerating supramolecluar assembly leads to the formation of nanofibers. The successful processing of the sericin into microparticles or nanofibers, which support the cell attachment, growth, and differentiation, makes it possible to apply sericin in the fabrication of tissue engineering scaffolds. This study not only broadens sericin application in the field of tissue engineering but also provides feedback information for the processing of sericin into useful scaffold forms.

■ ASSOCIATED CONTENT

Ⓢ Supporting Information

Supplementary Figure 1: DLS data showing average diameter of LS and HS solution. Supplementary Figure 2: Morphology and proliferation of MG-63 cells on electrospun mats. Supplementary Figure 3: ALP assay of MSCs cultured on the electrospun mats. Supplementary Figure 4: Real-time PCR analysis of the gene expression of osteocalcin (OCN). Supplementary Table 1: The amino acid composition analysis of LS and HS. This material is available free of charge via the Internet at http://pubs.acs.org.

■ AUTHOR INFORMATION

Corresponding Authors

*E-mail: cbmao@ou.edu (C.M.).
*E-mail: yangm@zju.edu.cn (M.Y.).

Author Contributions

§Mingying Yang and Yajun Shuai contributed equally to this work.

Notes

The authors declare no competing financial interest.

■ ACKNOWLEDGMENTS

M.Y. acknowledges the support of National High Technology Research and Development Program 863 (2013AA102507), Silkworm Industry Science and Technology Innovation Team (2011R50028), Zhejiang Provincial Natural Science Foundation of China (LZ12C17001), and National Natural Science Foundation of China (21172194 and 20804037). C.B.M. would like to thank the financial support from National Institutes of Health (EB015190 and HL092526), National Science Foundation (CBET-0854465, CMMI-1234957, CBET-0854414, and DMR-0847758), Department of Defense Peer Reviewed Medical Research Program (W81XWH-12-1-0384), Oklahoma Center for Adult Stem Cell Research (434003), and

Oklahoma Center for the Advancement of Science and Technology (HR11-006).

REFERENCES

(1) Heydarkhan-Hagvall, S.; Schenke-Layland, K.; Dhanasopon, A. P.; Rofail, F.; Smith, H.; Wu, B. M.; Shemin, R.; Beygui, R. E.; MacLellan, W. R. Three-dimensional Electrospun ECM-Based Hybrid Scaffolds for Cardiovascular Tissue Engineering. *Biomaterials* **2008**, *29*, 2907−2914.

(2) Yang, Q.; Peng, J.; Guo, Q.; Huang, J.; Zhang, L.; Yao, J.; Yang, F.; Wang, S.; Xu, W.; Wang, A. A Cartilage ECM-Derived 3-D Porous Acellular Matrix Scaffold for in vivo Cartilage Tissue Engineering with PKH26-Labeled Chondrogenic Bone Marrow-Derived Mesenchymal Stem Cells. *Biomaterials* **2008**, *29*, 2378−2387.

(3) Brown, R. A. Direct Collagen-Material Engineering for Tissue Fabrication. *Tissue Eng., Part A* **2013**, *19*, 1495−1498.

(4) Iafisco, M.; Quirici, N.; Foltran, I.; Rimondini, L. Electrospun Collagen Mimicking the Reconstituted Extracellular Matrix Improves Osteoblastic Differentiation onto Titanium Surfaces. *J. Nanosci. Nanotechnol.* **2013**, *13*, 4720−4726.

(5) Lee, S. S.; Huang, B. J.; Kaltz, S. R.; Sur, S.; Newcomb, C. J.; Stock, S. R.; Shah, R. N.; Stupp, S. I. Bone Regeneration with Low Dose BMP-2 Amplified by Biomimetic Supramolecular Nanofibers within Collagen Scaffolds. *Biomaterials* **2012**, *34*, 452−459.

(6) Marelli, B.; Achilli, M.; Alessandrino, A.; Freddi, G.; Tanzi, M. C.; Fare, S.; Mantovani, D. Collagen-Reinforced Electrospun Silk Fibroin Tubular Construct as Small Calibre Vascular Graft. *Macromol. Biosci.* **2012**, *12*, 1566−1574.

(7) Cao, B.; Mao, C. B. Oriented Nucleation of Hydroxylapatite Crystals on Spider Dragline Silks. *Langmuir* **2007**, *23*, 10701−10705.

(8) Cao, H.; Chen, X.; Yao, J. R.; Shao, Z. Z. Fabrication of an Alternative Regenerated Silk Fibroin Nanofiber and Carbonated Hydroxyapatite Multilayered Composite via Layer-By-Layer. *J. Mater. Sci.* **2013**, *48*, 150−155.

(9) Nishida, A.; Yamada, M.; Kanazawa, T.; Takashima, Y.; Ouchi, K.; Okada, H. Sustained-Release of Protein from Biodegradable Sericin Film, Gel and Sponge. *Int. J. Pharm.* **2011**, *407*, 44−52.

(10) Zhang, Y. Q. Applications of Natural Silk Protein Sericin in Biomaterials. *Biotechnol. Adv.* **2002**, *20*, 91−100.

(11) Zhaorigetu, S.; Sasaki, M.; Kato, N. Consumption of Sericin Suppresses Colon Oxidative Stress and Aberrant Crypt Foci in 1,2-dimethylhydrazine-Treated Rats by Colon Undigested Sericin. *J. Nutr. Sci. Vitaminol.* **2007**, *53*, 297−300.

(12) Kato, N.; Sato, S.; Yamanaka, A.; Yamada, H.; Fuwa, N.; Nomura, M. Silk Protein, Sericin, Inhibits Lipid Peroxidation and Tyrosinase Activity. *Biosci. Biotechnol. Biochem.* **1998**, *62*, 145−147.

(13) Zhang, Y. Q.; Tao, M. L.; Shen, W. D.; Zhou, Y. Z.; Ding, Y.; Ma, Y.; Zhou, W. L. Immobilization of L-asparaginase on the Microparticles of the Natural Silk Sericin Protein and its Characters. *Biomaterials* **2004**, *25*, 3751−3759.

(14) Sasaki, M.; Kato, N.; Watanabe, H.; Yamada, H. Silk Protein, Sericin, Suppresses Colon Carcinogenesis Induced by 1,2-dimethylhydrazine in Mice. *Oncol. Rep.* **2000**, *7*, 1049−1052.

(15) Sasaki, M.; Yamada, H.; Kato, N. Consumption of Silk Protein, Sericin, Elevates Intestinal Absorption of Zinc, Iron, Magnesium and Calcium in Rats. *Nutr. Res. (N.Y.)* **2000**, *20*, 1505−1511.

(16) Wang, Y.; Kim, H. J.; Vunjak-Novakovic, G.; Kaplan, D. L. Stem Cell-Based Tissue Engineering with Silk Biomaterials. *Biomaterials* **2006**, *27*, 6064−6082.

(17) Sofia, S.; McCarthy, M. B.; Gronowicz, G.; Kaplan, D. L. Functionalized Silk-Based Biomaterials for Bone Formation. *J. Biomed. Mater. Res.* **2001**, *54*, 139−148.

(18) Mandal, B. B.; Kundu, S. C. Cell Proliferation and Migration in Silk Fibroin 3D scaffolds. *Biomaterials* **2009**, *30*, 2956−2965.

(19) Zhang, X. H.; Rahman Khan, M. M.; Yamamoto, T.; Tsukada, M.; Morikawa, H. Fabrication of Silk Sericin Nanofibers from a Silk Sericin-hope Cocoon with Electrospinning Method. *Int. J. Biol. Macromol.* **2012**, *50*, 337−347.

(20) Rahman Khan, M. M.; Tsukada, M.; Zhang, X. H.; Morikawa, H. Preparation and Characterization of Electrospun Nanofibers Based on Silk Sericin Powders. *J. Mater. Sci.* **2013**, *48*, 3731−3736.

(21) Yang, M. Y.; Tanaka, C.; Yamauchi, K.; Ohgo, K.; Kurokawa, M.; Asakura, T. Silklike Materials Constructed from Sequences of *Bombyx mori* Silk Fibroin, Fibronectin, and Elastin. *J. Biomed. Mater. Res., Part A* **2008**, *84*, 353−363.

(22) Yang, M. Y.; Kawamura, J.; Zhu, Z. H.; Yamauchi, K.; Asakura, T. Development of Silk-Like Materials Based on *Bombyx mori* and *Nephila clavipes* Dragline Silk Fibroins. *Polymer* **2009**, *50*, 117−124.

(23) Baker, B. M.; Shah, R. P.; Silverstein, A. M.; Esterhai, J. L.; Burdick, J. A.; Mauck, R. L. Sacrificial Nanofibrous Composites Provide Instruction Without Impediment and Enable Functional Tissue Formation. *Proc. Natl. Acad. Sci. U.S.A.* **2012**, *109*, 14176−14181.

(24) Li, X.; Xie, J.; Yuan, X.; Xia, Y. Coating Electrospun Poly (ε-caprolactone) Fibers with Gelatin and Calcium Phosphate and Their Use as Biomimetic Scaffolds for Bone Tissue Engineering. *Langmuir* **2008**, *24*, 14145−14150.

(25) Abdel-Fattah, W. I.; Jiang, T.; El-Bassyouni, G.-T.; Laurencin, C. T. Synthesis, Characterization of Chitosans and Fabrication of Sintered Chitosan Microsphere Matrices for Bone Tissue Engineering. *Acta. Biomater.* **2007**, *3*, 503−514.

(26) Borden, M.; Attawia, M.; Khan, Y.; Laurencin, C. T. Tissue Engineered Microsphere-Based Matrices for Bone Repair: Design and Evaluation. *Biomaterials* **2002**, *23*, 551−559.

(27) Wu, J. H.; Wang, Z.; Xu, S. Y. Preparation and Characterization of Sericin Powder Extracted from Silk Industry Wastewater. *Food Chem.* **2007**, *103*, 1255−1262.

(28) Ha, S. W.; Asakura, T.; Kishore, R. Distinctive Influence of Two Hexafluoro Solvents on the Structural Stabilization of *Bombyx mori* Silk Fibroin Protein and Its Derived Peptides: ^{13}C NMR and CD Studies. *Biomacromolecules* **2006**, *7*, 18−23.

(29) Takeuchi, A.; Ohtsuki, C.; Miyazaki, T.; Kamitakahara, M.; Ogata, S.; Yamazaki, M.; Furutani, Y.; Kinoshita, H.; Tanihara, M. Heterogeneous Nucleation of Hydroxyapatite on Protein: Structural Effect of Silk Sericin. *J. R. Soc. Interface* **2005**, *2*, 373−378.

(30) Cho, K. Y.; Moon, J. Y.; Lee, Y. W.; Lee, K. G.; Yeo, J. H.; Kweon, H. Y.; Kim, K. H.; Cho, C. S. Preparation of Self-Assembled Silk Sericin Nanoparticles. *Int. J. Biol. Macromol.* **2003**, *32*, 36−42.

(31) Dash, R.; Mukherjee, S.; Kundu, S. C. Isolation, Purification and Characterization of Silk Protein Sericin from Cocoon Peduncles of Tropical Tasar Silkworm, Antheraea mylitta. *Int. J. Biol. Macromol.* **2006**, *38*, 255−258.

(32) Yang, M. Y.; He, W.; Shuai, Y. J.; Min, S. J.; Zhu, L. J. Nucleation of Hydroxyapatite Crystals by Self-Assembled Bombyx mori Silk Fibroin. *J. Polym. Sci., Part B: Polym. Phys.* **2013**, *51*, 742−748.

(33) Lee, K.; Kweon, H.; Yeo, J. H.; Woo, S. O.; Lee, Y. W.; Cho, C. S.; Kim, K. H.; Park, Y. H. Effect of Methyl Alcohol on the Morphology and Conformational Characteristics of Silk Sericin. *Int. J. Biol. Macromol.* **2003**, *33*, 75−80.

(34) Wang, J.; Wang, L.; Li, X.; Mao, C. B. Virus Activated Artificial ECM Induces the Osteogenic Differentiation of Mesenchymal Stem Cells without Osteogenic Supplements. *Sci. Rep.* **2013**, *3*, 1242.

(35) Zhu, H.; Cao, B.; Zhen, Z.; Laxmi, A.; Li, D.; Liu, S.; Mao, C. B. Controlled Growth and Differentiation of Mesenchymal Stem Cells on Grooved Films Assembled from Monodisperse Biological Nanofibers with Genetically Tunable Surface Chemistries. *Biomaterials* **2011**, *32*, 4744−4752.